SciForschen
Open HUB for Scientific Research

ISSN: 2470-3206

International Journal of Nanomedicine and Nanosurgery

Research Article | Volume: 2.3 | Open Access

Quantitative Evaluation of Tumor Early Response to Magnetic Hyperthermia combined with Vascular Disrupting Therapy using Magnetic Particle Imaging

Tomomi Kuboyabu, Mikiko Yamawaki, Marina Aoki, Akiko Ohki and Kenya Murase*

Department of Medical Physics and Engineering, Division of Medical Technology and Science, Faculty of Health Science, Graduate School of Medicine, Osaka University, Suita, Osaka, Japan

***Corresponding author:** Kenya Murase, Ph.D, Department of Medical Physics and Engineering, Division of Medical Technology and Science, Faculty of Health Science, Graduate School of Medicine, Osaka University 1-7 Yamadaoka, Suita, Osaka 565-0871, Japan, Tel: 81-6-6879-2571; Fax: 81-6-6879-2571; **E-mail:** murase@sahs.med.osaka-u.ac.jp

Received date: 17 May 2016; **Accepted date:** 03 Jun 2016; **Published date:** 08 Jun 2016.

Citation: Kuboyabu T, Yamawaki M, Aoki M, Ohki A, Murase K (2016) Quantitative Evaluation of Tumor Early Response to Magnetic Hyperthermia combined with Vascular Disrupting Therapy using Magnetic Particle Imaging. Int J Nanomed Nanosurg 2(3): doi http://dx.doi.org/10.16966/2470-3206.114

Abstract

Purpose: Magnetic hyperthermia treatment (MHT) is a strategy for cancer therapy using the temperature rise of magnetic nanoparticles (MNPs) under an alternating magnetic field (AMF). Vascular disrupting agents (VDAs) selectively damage the endothelial cells of tumor blood vessels, inducing reduction of tumor blood flow and necrosis of tumor cells. The purpose of this study was to quantitatively evaluate the tumor early response to MHT combined with VDA (MHT+VDA) in comparison with that to MHT alone using magnetic particle imaging (MPI).

Materials and methods: Colon-26 cells (1×10^6 cells) were implanted into the backs of eight-week-old male BALB/c mice. When the tumor volume reached approximately 100 mm^3, the mice were divided into MHT+VDA (n=12) and MHT groups (n=11). In the MHT+VDA group, VDA (Trisenox®) was injected intraperitoneally at a single dose of 4 mg/kg. Two hours after the injection of VDA, MNPs (Resovist®) with an iron (Fe) concentration of 250 mM (14.0 mg Fe/mL) were directly injected into the tumor and MHT was performed for 20 min using an AMF (frequency: 600 kHz and peak amplitude: 3.5 kA/m). In the MHT group, only MHT was performed. In both groups, MPI images were obtained using our MPI scanner immediately before MHT, immediately after MHT, and 1, 3, 7, and 14 days after MHT. After the MPI studies, we drew a region of interest (ROI) on the tumor in the MPI image and calculated the average, maximum, and total MPI values, and the number of pixels by taking the threshold value for extracting the contour of the tumor as 40% of the maximum MPI value (pixel value) within the ROI. We also measured the relative tumor volume growth (RTVG) defined by $(V-V_0)/V_0$, where V_0 and V are the tumor volumes immediately before and after MHT, respectively.

Results: The RTVG value in the MHT+VDA group was significantly lower than that in the MHT group 1 and 2 days after MHT. The average and maximum MPI values in the MHT+VDA group were significantly higher than those in the MHT group 3 and 7 days after MHT, indicating that the retention of MNPs in the tumor was significantly enhanced by the use of VDA.

Conclusions: Our results suggest that VDA is useful for enhancing the therapeutic effect of MHT at the early stage after VDA injection, and for enhancing the retention of MNPs in the tumor, which will be useful for repeated applications of MHT. Our results also suggest that MPI is useful for quantitatively evaluating the tumor response to therapeutic agents such as VDA.

Keywords: Magnetic particle imaging; Magnetic hyperthermia; Vascular disrupting therapy; Tumor-bearing mice; Tumor early response

Introduction

The use of vascular disrupting agents (VDAs) is one of the therapeutic approaches that target already-established tumor vasculatures of solid tumors [1]. There are two classes of VDAs, i.e., tubulin-binding VDAs and flavonoid VDAs [1]. Tubulin-binding VDAs selectively disrupt the cytoskeleton of proliferating tumor blood vessel endothelial cells. Flavonoid VDAs induce apoptosis in tumor blood vessel endothelial cells. Arsenic trioxide has been used clinically as an effective agent for acute promyelocytic leukemia [2]. It has been reported that arsenic trioxide has an antivascular effect on solid tumors as a tubulin-binding VDA [3] and induces vascular shut down and necrosis in the tumor [4].

Hyperthermia is one of the approaches to cancer therapy, and is based on the fact that cancer cells are more sensitive to heat than normal tissues. The most commonly used heating method in the clinical setting is capacitive heating that employs a radiofrequency (RF) electric field [5]. The therapeutic effect of hyperthermia depends on the temperature and the heating duration. The cell-killing mechanism of hyperthermia is linked to activation of the immune system [6] and its efficacy increases dramatically at temperatures above 42.5°C. The heating duration can be shortened with each 1°C temperature increase to give an equivalent cell-killing effect [7]. The therapeutic effect of hyperthermia can be enhanced by combining it with radiotherapy, chemotherapy and/or immunotherapy [8-10]. Recently, hyperthermia combined with VDA has been introduced [11] and it has been reported that arsenic trioxide can increase tumor thermo-sensitivity and heat-induced tumor growth delay [11].

Magnetic hyperthermia treatment (MHT) is one of the hyperthermia treatments and employs the temperature rise of magnetic nanoparticles (MNPs) under an alternating magnetic field (AMF). MNPs generate heat through hysteresis loss and/or relaxational loss due to Nèel and Brownian relaxations when exposed to AMF [12]. Although conventional hyperthermia treatments such as RF-capacitive heating [5] damage not only cancer cells but also normal tissues, MHT can selectively heat tumor cells without damaging normal tissues [13]. In order to enhance the

therapeutic effect of MHT, it is necessary to deliver and accumulate as many MNPs as possible into the tumor tissues [12].

Magnetic particle imaging (MPI) is an imaging modality that was introduced in 2005 [14]. MPI uses the nonlinear response of MNPs to an external oscillating magnetic field and is capable of imaging the spatial distribution of MNPs such as superparamagnetic iron oxide with high sensitivity and high spatial resolution [14].

The purpose of this study was to quantitatively evaluate the tumor early response to MHT combined with VDA in comparison with that to MHT alone using MPI.

Materials and Methods

System for magnetic particle imaging

The details of our MPI system are described in our previous reports [15-17]. In brief, a drive magnetic field was generated using an excitation coil (solenoid coil 100 mm in length, 80 mm in inner diameter, and 110 mm in outer diameter). AC power was supplied to the excitation coil by a programmable power supply (EC1000S, NF Co., Yokohama, Japan), and was controlled using a sinusoidal wave generated by a digital function generator (DF1906, NF Co., Yokohama, Japan). The frequency and peak-to-peak strength of the drive magnetic field were taken as 400 Hz and 20 mT, respectively [15]. The signal generated by MNPs was received by a gradiometer coil (50 mm in length, 35 mm in inner diameter, and 40 mm in outer diameter), and the third-harmonic signal was extracted using a preamplifier (T-AMP03HC, Turtle Industry Co., Ibaragi, Japan) and a lock-in amplifier (LI5640, NF Co., Yokohama, Japan). The output of the lock-in amplifier was converted to digital data by a personal computer connected to a multifunction data acquisition device with a universal serial bus port (USB-6212, National Instruments Co., TX, USA). The sampling time was taken as 10 msec. When measuring signals using the gradiometer coil, a sample was placed 12.5 mm (i.e., one quarter of the coil length) from the center of the gradiometer coil and the coil, including the sample, was moved such that the center of the sample coincided with the position of the field-free line. The selection magnetic field was generated by two opposing neodymium magnets (Neomax Engineering Co., Gunma, Japan). The field-free line can be generated at the center of the two neodymium magnets.

To acquire projection data for image reconstruction, a sample in the receiving coil was automatically rotated around the z-axis over 180° in steps of 5° and translated in the x-direction from −16 mm to 16 mm in steps of 1 mm using an XYZ-axes rotary stage (HPS80-50X-M5, Sigma Koki Co., Tokyo, Japan) controlled using LabVIEW (National Instruments Co., TX, USA). Data acquisition took about 12 min. Each projection data set was then transformed into 64 bins by linear interpolation. Both the inhomogeneous sensitivity of the receiving coil and feed-through interference were corrected using the method described in [16]. Transverse images were reconstructed from the projection data using the maximum likelihood-expectation maximization (ML-EM) algorithm over 15 iterations, in which the initial concentration of MNPs was assumed to be uniform [15,17]. In this study, the MPI value was defined as the pixel value of the transverse MPI image reconstructed from the third-harmonic signals.

Apparatus for magnetic hyperthermia treatment

The details of our apparatus for MHT are described in our previous report [18]. In brief, the coil for generating an AMF consists of 19-turned loops (6.5 cm in diameter and 10 cm in length) of copper pipe (5 mm in diameter) and is cooled by water to ensure constant temperature and impedance. The coil is connected to a high-frequency power supply (T162-5723BHE, Thamway Co., Ltd, Shizuoka, Japan) and a manual-matching unit (T020-5723AHE, Thamway Co., Ltd, Shizuoka, Japan). The peak amplitude of the AMF generated in the coil can be controlled by changing the output of the power supply.

Animals and tumor model

All animal experiments were approved by the animal ethics committee at Osaka University School of Medicine. Seven-week-old male BALB/c mice were purchased from Charles River Laboratories Japan, Inc. (Yokohama, Japan), and were habituated to the rearing environment for one week before the experiment. The animals had free access to food and water, and were kept under standard laboratory conditions of 23°C room temperature and around 50% humidity.

Colon-26 (a mouse cell line derived from rectal cancer) cells (Riken BioResource Center, Ibaragi, Japan) were cultured in RPMI-1640 medium (Mediatech Inc., VA, USA) supplemented with 10% fetal bovine serum (FBS) (Biowest, Nuaillé, France) and 1% Penicillin-Streptomycin (Nacalai Tesque Inc., Kyoto, Japan). All cultures were incubated in a humidified atmosphere containing 5% CO_2 at 37°C. Cells were trypsinized with 0.25% trypsin in ethylenediaminetetraacetic acid (EDTA) (Nacalai Tesque Inc., Kyoto, Japan) and resuspended in phosphate-buffered saline (PBS) at 1×10^6 cells/100 μL.

The cells (1×10^6 cells) were implanted into the backs of 8-week-old mice on the same day and under the same conditions. During the implantation, the mice were anesthetized by intraperitoneal injection of pentobarbital sodium (Somnopentyl, Kyoritsu Seiyaku Co., Tokyo, Japan) at a dose of 0.012 mL/g body weight (BW) (10-fold dilution).

Vascular disrupting agent

In this study, arsenic trioxide (Trisenox®, Nippon Shinyaku Co., Ltd., Kyoto, Japan) was used as VDA. When investigating the effect of VDA, mice were intraperitoneally injected with Trisenox® at a single dose of 4 mg/kg BW.

Magnetic nanoparticles

In this study, Resovist® (FUJIFILM RI Pharma Co., Ltd., Tokyo, Japan) was used as the source of MNPs, because it is commercially available and has been approved for clinical use in Japan. Resovist® consists of MNPs (maghemite, γ-Fe_2O_3) coated with carboxydextran. It is an organ-specific contrast agent for magnetic resonance imaging (MRI), used especially for the detection of hepatocellular carcinoma and liver metastasis [18]. According to Biederer et al. [19], the mean and standard deviation of the particle size of Resovist® are 15.2 nm and 3.21 nm, respectively.

Tumor blood flow measurement

Tumor blood flow was measured using a laser Doppler flow meter (FLO-N1, OMEGAWAVE Inc., Tokyo, Japan). When measuring the tumor blood flow, each tumor-bearing mouse was fixed on a board with surgical tape under anesthesia and a probe was set approximately 5 mm above the tumor surface. Continuous recordings were initiated 10 min before the intraperitoneal injection of VDA (n=4) or PBS (n=3) to obtain the baseline blood flow and lasted for 2 hours.

Study protocol

Figure 1 shows the time schedule for data acquisition in the present study. When the tumor volume had grown to approximately 100 mm^3, mice were divided into two groups. One group consisted of mice treated with MHT in combination with VDA (MHT+VDA group, n=12), whereas the other group consisted of mice treated with MHT alone (MHT group, n=11). For comparison, we also used the data of the mice without MHT and VDA as control (control group, n=9). In the MHT+VDA group, VDA was intraperitoneally injected in a single dose of 4 mg/kg BW. Two hours after the injection of VDA, Resovist® (0.2 mL of stock solution diluted in

PBS) with an iron (Fe) concentration of 250 mM (14.0 mg Fe/mL) was directly injected into the tumor under anesthesia. Fifteen min after the injection of Resovist®, each mouse was placed in the holder and set in the coil for generating an AMF. MHT was performed by applying an AMF at a frequency of 600 kHz and peak amplitude of 3.5 kA/m [18] for 20 min. In the MHT group, only MHT was performed without the injection of VDA.

Each tumor-bearing mouse was scanned 6 times using our MPI scanner [15]; immediately before MHT, immediately after MHT, and 1, 3, 7, and 14 days after MHT (Figure 1). After the MPI studies, X-ray CT images were obtained using a 4-row multi-slice CT scanner (Asteion, Toshiba Medical Systems Co., Tochigi, Japan) with a tube voltage of 120 kV, a tube current of 210 mA, and a slice thickness of 0.5 mm. The MPI image was co-registered to the X-ray CT image to confirm the spatial distribution of Resovist® in the tumor-bearing mouse using the method described in [20]. It should be noted that the X-ray CT image after the first MPI study was substituted by that obtained after the second MPI study.

Histological study

Separately from the above studies, mice were purchased for histological studies and were implanted with colon-26 cells in the same manner as described above. The tumor-bearing mice were sacrificed and the tumors were removed immediately after MHT, and 3, 7, and 14 days after MHT (n=3 each). The tumor tissues were fixed in a 7.5% formaldehyde neutral buffered solution (Sigma-Aldrich Japan Co., Ltd., Tokyo, Japan), dehydrated, and embedded in paraffin. They were then sectioned at a thickness of 3 μm on a microtome and stained with hematoxylin and eosin (H&E). The histological images were acquired with a microscope (ECLIPSE80i, NIKON Co. Ltd., Tokyo, Japan) at a magnification of 20 and imaging software (NIS-Elements D, NIKON Co. Ltd., Tokyo, Japan).

Data analysis

The dimensions of the tumors in all mice were measured with a caliper every day until 14 days after MHT. The tumor volume (V) was calculated from $V = (\pi/6) \times Lx \times Ly \times Lz$, where Lx, Ly, and Lz represent the vertical diameter, the horizontal diameter, and the height in mm, respectively. The relative tumor volume growth (RTVG) was also calculated from $(V-V_0)/V_0$, where V_0 represents the tumor volume immediately before MHT. In this study, the RTVG value was used as an indicator of the therapeutic effect of MHT+VDA or MHT.

After the MPI studies, we drew a region of interest (ROI) on the tumor in the MPI image and calculated the average, maximum, and total MPI values and the number of pixels within the ROI by taking the threshold value for extracting the contour of the tumor as 40% of the maximum MPI value within the ROI. The total MPI value is equal to the product of the average MPI value and the number of pixels.

Statistical analysis

The tumor blood flow, RTVG value, average, maximum, and total MPI values and the number of pixels within the ROI were expressed as the mean ± standard error (SE). The one-way analysis of variance (ANOVA) was used for comparison among three groups and statistical significance was determined by Tukey's multiple comparison tests. The Student's t test or Welch's t test (two-tailed) was used for comparisons between two groups. A P value less than 0.05 was considered statistically significant.

Results

Figure 2 shows the time courses of the tumor blood flow measured using a laser Doppler flow meter in the mice injected with VDA (●, n=4) and PBS (▪, n=3). In the mice injected with PBS, the tumor blood flow slightly increased up to approximately 10 min and plateaued for approximately 30 min. It then decreased gradually up to 70 min and became stable thereafter. In the mice injected with VDA, the tumor blood flow decreased up to approximately 30 min and then increased gradually to the initial blood flow level approximately 100 min after VDA injection. The tumor blood flow in the mice injected with VDA was significantly lower than that in the mice injected with PBS 15 to 50 min after the injection of VDA or PBS.

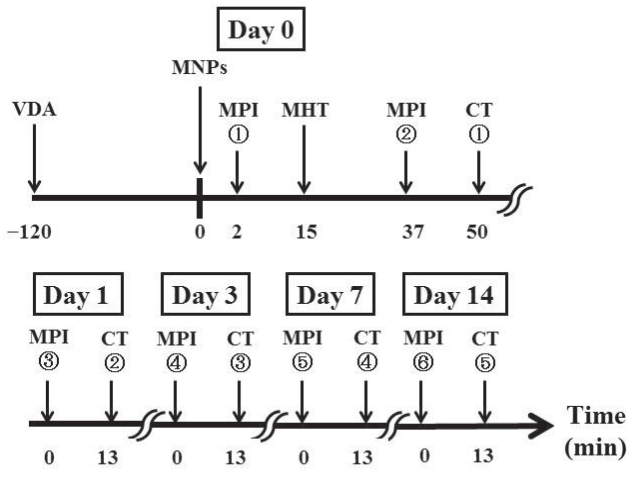

Figure 1: Time schedule for data acquisition in the present study. VDA: vascular disrupting agent, MNPs: magnetic nanoparticles, MPI: magnetic particle imaging, CT: X-ray computed tomography, and MHT: magnetic hyperthermia treatment. Note that we used arsenic trioxide (Trisenox®) as the VDA and injected it into mice intraperitoneally, whereas we used Resovist® as the source of MNPs and injected it directly into the tumor.

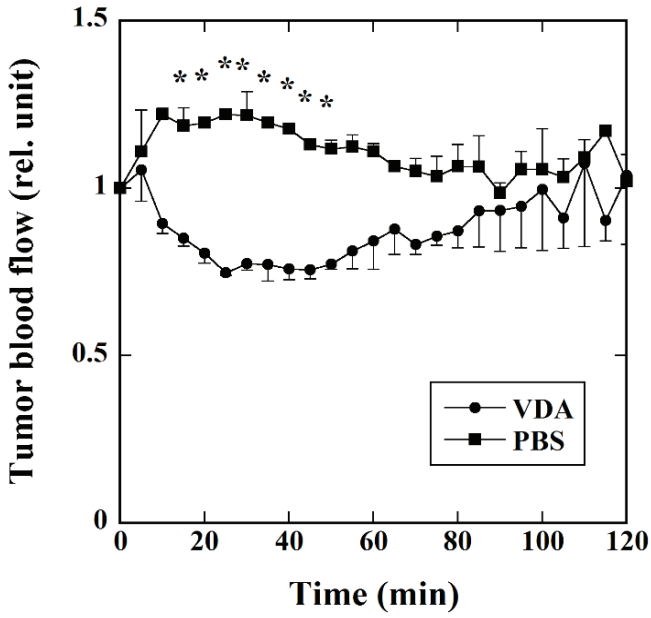

Figure 2: Time courses of the tumor blood flow measured using a laser Doppler flow meter in mice injected with VDA (●, n=4) and phosphate-buffered saline (PBS) (■, n=3). The blood flow values 5 to 120 min after the injection of VDA or PBS was normalized by the average blood flow value for 10 min before the injection. *: P<0.05.

Figure 3 shows the time courses of the RTVG values in the MHT+VDA (●, n=12), MHT (▪, n=11), and the control groups (▲, n=9). The RTVG value in the MHT+VDA group was significantly lower than that in the MHT group 1 and 2 days after MHT. The RTVG value in the MHT+VDA group was also significantly lower than that in the control group 2 to 4 days after MHT.

Figure 4 shows the MPI images superimposed on the X-ray CT images immediately before MHT (a), immediately after MHT (b), and 1 day (c), 3 days (d), 7 days (e), and 14 days after MHT (f). The upper and lower panels show those in the MHT+VDA and MHT groups, respectively. As shown in figure 4, the MPI value tended to decrease and the spatial distribution of MNPs changed with time in both groups. It was visually confirmed that the MPI value in the MHT+VDA group tended to be higher than that in the MHT group 1 to 14 days after MHT.

Figure 5 shows the temporal changes of the average MPI value (a), maximum MPI value (b), number of pixels within the ROI (c), and total MPI value (d). The closed and open bars show those in the MHT+VDA (n=12) and MHT groups (n=11), respectively. The average and maximum MPI values in the MHT+VDA group were significantly higher than those in the MHT group 3 and 7 days after MHT. The average and maximum MPI values in the MHT+VDA group also tended to be higher than those in the MHT group 14 days after MHT. In these cases, the *P* values were 0.065 and 0.075 for the average and maximum MPI values, respectively. Although the number of pixels within the ROI tended to increase with time in both groups, and the total MPI value in the MHT+VDA group tended to be higher than that in the MHT group 3 to 14 days after MHT, they did not reach statistical significance due to large scattering of the data.

Figure 6 shows typical H&E stain images in the MHT+VDA (left column) and MHT groups (right column) immediately after MHT (top row), and 3 days (second row), 7 days (third row), and 14 days after MHT (bottom row). As shown in figure 6, the necrotic area (shown by N) in the MHT+VDA group was larger than that in the MHT group in all cases.

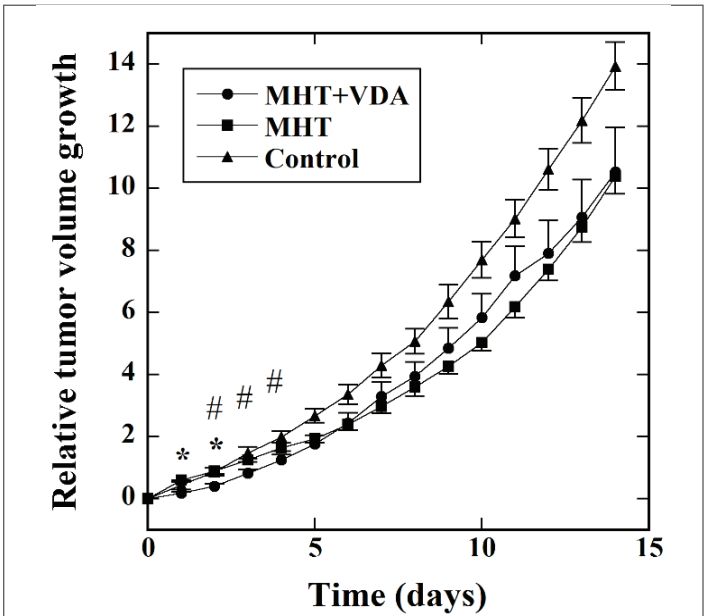

Figure 3: Time courses of the relative tumor volume growth (RTVG) values in the MHT+VDA (●, n=12), MHT (■, n=11), and control groups (▲, n=9). The mice in the MHT+VDA and MHT groups were treated with MHT combined with VDA and MHT alone, respectively, whereas those in the control group were not treated with MHT and VDA. *: *P*<0.05 between the MHT+VDA and MHT groups and #: *P*<0.05 between the MHT+VDA and control groups.

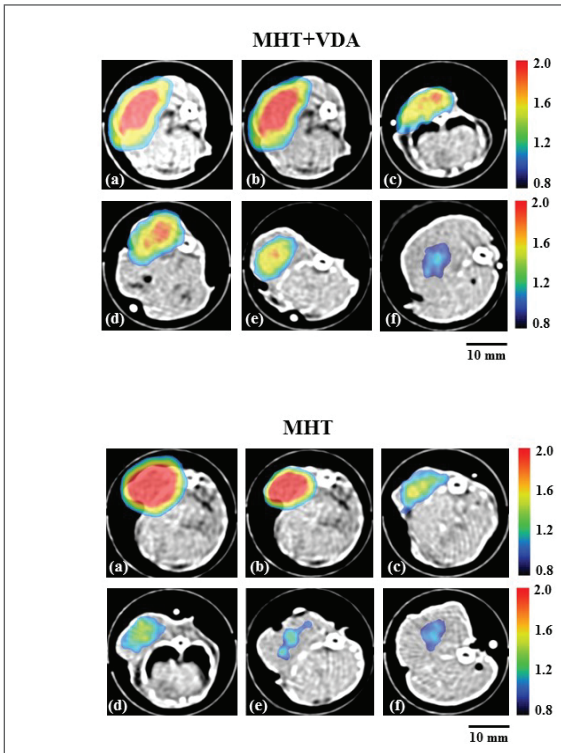

Figure 4: MPI images superimposed on X-ray CT images in the MHT+VDA (upper panels) and MHT groups (lower panels) immediately before MHT **(a)**, immediately after MHT **(b)**, and 1 day **(c)**, 3 days **(d)**, 7 days **(e)**, and 14 days after MHT **(f)**. Scale bar = 10 mm.

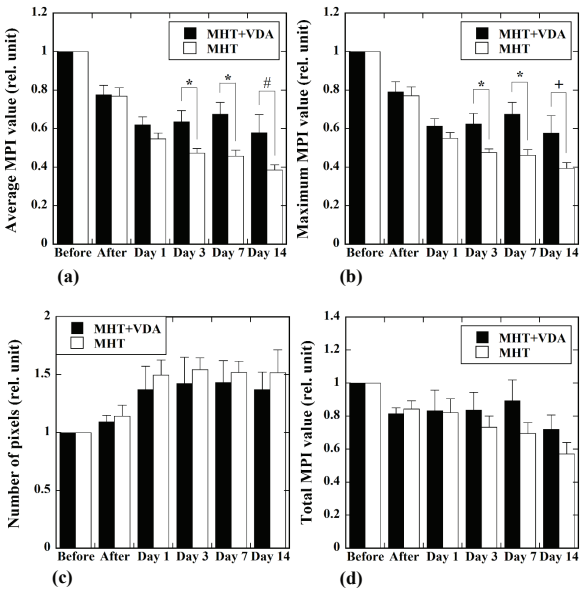

Figure 5: Temporal changes of the average MPI value **(a)**, maximum MPI value **(b)**, number of pixels within the region of interest (ROI) **(c)**, and total MPI value **(d)**. The closed and open bars represent cases for the MHT+VDA (n=12) and MHT groups (n=11), respectively. Each bar and error bar represent the mean and standard error, respectively. The values immediately after MHT, and 1, 3, 7, and 14 days after MHT were normalized by those immediately before MHT. *: *P*<0.05, #: *P*=0.065, and +: *P*=0.075.

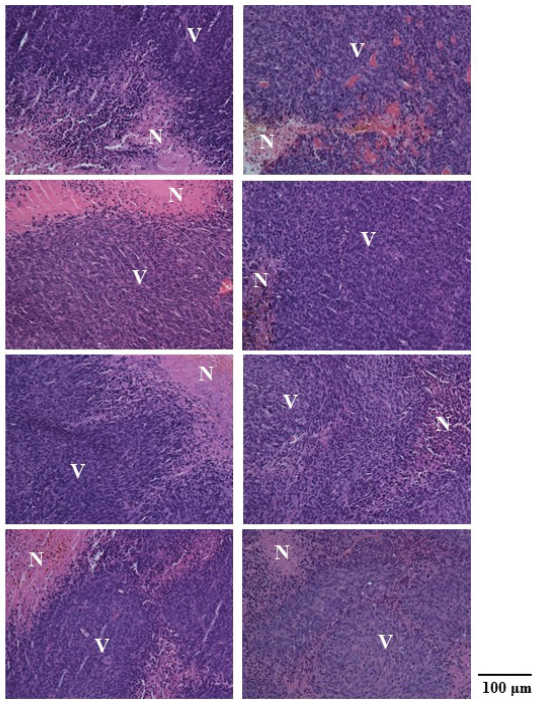

Figure 6: Hematoxylin and eosin (H&E) stain images in the MHT+VDA (left column) and MHT groups (right column) immediately after MHT (top row), and 3 days (second row), 7 days (third row), and 14 days after MHT (bottom row). Magnification, X20. N: necrotic area and V: viable area. Scale bar=100 µm.

Discussion

In this study, we investigated the tumor response to MHT+VDA in comparison with that to MHT alone by quantitatively evaluating the temporal change of the MNPs in the tumors of tumor-bearing mice using MPI. We also investigated the synergistic effect of VDA on MHT in terms of RTVG. As previously described, we used Trisenox® at a dose of 4 mg/kg BW as VDA and Resovist® with an iron concentration of 250 mM as the source of MNPs. In this study, we injected Trisenox® into each tumor-bearing mouse intraperitoneally only once, whereas we injected Resovist® directly into the tumor and MHT was performed only once for each mouse. This is mainly because the purpose of this study was to quantitatively evaluate the tumor response to MHT+VDA in comparison with that to MHT alone using MPI, rather than to search for a method for enhancing the therapeutic effect of MHT.

As shown in figure 3, the RTVG value in the MHT+VDA group was significantly lower than that in the MHT group 1 and 2 days after MHT. It was also significantly lower than the RTVG value in the control group 2 to 4 days after MHT. However, there was no significant difference in the RTVG value between the MHT and control groups. In our previous studies [20,21], when an AMF with the same frequency and peak amplitude as those in this study was applied to the tumor injected with 250 mM Resovist® for 20 min, the temperature in the tumor rose to around 41°C. It has been reported that mild hyperthermia at approximately 40°C decreases the induction of cytotoxicity and endoplasmic reticulum (ER) stress and rather protects cells against ER stress-induced apoptosis [22]. In contrast, arsenic trioxide is useful for decreasing tumor blood perfusion and inhibiting the heat dissipation and can increase tumor thermo-sensitivity at temperatures as low as 41.5°C [11]. Thus, we can expect a synergistic effect of VDA in mild hyperthermia when combined with MHT.

In our histological study, the necrotic area in the MHT+VDA group was larger than that in the MHT group (Figure 6), indicating that VDA is useful for enhancing the necrosis of the tumor. Thus, our results (Figure 6) suggest that MHT combined with VDA is more effective for delaying the tumor growth than MHT alone. Although the therapeutic effect of VDA was observed in terms of the tumor volume growth, this effect was limited to the early stage after VDA injection and disappeared 3 days or more after MHT (Figure 3). VDAs induce the disruption of abnormal peripheral blood vessels and central necrosis of tumors [1]. As described by Tozer et al. [23], a common feature of the vascular effects of VDAs is the sparing of tumor cells in the peripheral rim; the tumor cells in this region survive and proliferate because they receive oxygen and nutrients from surrounding normal tissue. This feature of VDAs appears to be the main reason why the effect of VDA on the tumor volume growth is limited to the early stage after VDA injection (Figure 3).

As shown in figure 2, the tumor blood flow in the mice injected with VDA significantly decreased in comparison with that in the mice injected with PBS 15 to 50 min after the injection of VDA or PBS. Approximately 2 hours after the injection of VDA, however, the tumor blood flow recovered to the initial blood flow level. In this study, MHT was started 2 hours and 15 min after the injection of VDA (Figure 1). Thus, the results shown in figure 2 suggest that there is almost no effect of VDA on the tumor blood perfusion during MHT. This may also be one of the reasons why the effect of VDA on the tumor volume growth is limited to the early stage after VDA injection (Figure 3). It might be necessary to shorten the period between the time of VDA injection and the start time of MHT to enhance the synergistic effect of VDA. In addition to the timing of VDA injection, the reduction of the tumor blood flow and induction of the necrosis in the tumor depend on the injected dose of VDA [24]. If we used Trisenox® at a higher dose than that adopted in this study (4 mg/kg BW) and/or injected multiple doses of Trisenox®, the therapeutic effect of VDA might be higher than that in this study. However, it has been shown that the injection of high-dose arsenic trioxide induces systemic side effects on the heart, lung, spleen, liver, kidney or brain [25]. Alternatively, the inhibition of nitric oxide synthase (NOS) induces the reduction of tumor blood flow [26] and enhances the tumor vascular damaging effect of VDA [27]. Thus, the combination of arsenic trioxide and a NOS inhibitor may be more effective for improving the therapeutic effect than the use of high-dose arsenic trioxide. These studies are currently in progress.

The MPI images superimposed on the X-ray CT images were useful for visualizing the temporal change of MNPs in the tumor (Figure 4). As shown in figure 4, the MPI pixel values tended to decrease and the spatial distribution of MNPs changed with time in both the MHT+VDA and MHT groups. In addition, the MPI pixel values in the MHT+VDA group tended to be higher than those in the MHT group. To quantitatively evaluate the temporal change of MNPs in the tumor, we calculated the average, maximum, and total MPI values, and the number of pixels within the ROI drawn on the tumor in the MPI image immediately before MHT, immediately after MHT, and 1, 3, 7, and 14 days after MHT (Figure 5). We previously reported an excellent linear correlation between the average MPI value and the iron concentration of Resovist® in phantom studies [20]. From this finding, it appears that the change in the average MPI value corresponds to that in the amount of MNPs per voxel and the change in the total MPI value corresponds to that in the total amount of MNPs in the selected slice of the tumor, whereas the change in the number of pixels corresponds to that in the distributed area of MNPs. As shown in figure 5, the average and maximum MPI values in the MHT+VDA group were significantly higher than those in the MHT group 3 and 7 days after MHT and the total MPI value in the MHT+VDA group tended to be higher than that in the MHT group 3 to 14 days after MHT. These results suggest that when VDA was used, the MNPs injected directly into the tumor were confined to the tumor and their dispersion within the tumor was

suppressed due to the vascular disrupting effect of VDA 3 to 7 days after MHT. The fact that VDA significantly enhances the retention of MNPs in the tumor (Figure 5) will be useful when considering the repeated applications of MHT to enhance its therapeutic effect.

As described above, we demonstrated that MPI allows us to quantitatively evaluate the tumor response to MHT or MHT+VDA using values such as the average and maximum MPI values within the ROI (Figure 5). To the best of our knowledge, this is the first report to show that MPI is useful for evaluating the tumor response to therapeutic agents such as VDA. We previously reported that the average MPI value is significantly inversely correlated with the RTVG value and will be useful for predicting the therapeutic effect and treatment planning of MHT [20,21]. We believe that MPI can also be applied to prediction of the therapeutic effect and treatment planning of MHT+VDA.

Other methods for evaluating the tumor early response to VDA are positron emission tomography (PET) and dynamic contrast-enhanced MRI (DCE-MRI) [28,29]. Guo et al. [28] reported that the retention of radiotracers in the tumor measured by PET was significantly enhanced by injection of VDA 1 to 3 days after the intravenous injection of radiotracers. Gao et al. [29] reported that the retention of gadolinium-diethylenetriamine pentaacetic acid (Gd-DTPA) in a tumor measured by DCE-MRI was significantly enhanced due to the injection of VDA 6 to 24 hours after the intravenous injection of Gd-DTPA. In this study, MNPs were directly injected into the tumor as previously described and the retention of MNPs in the tumor was significantly enhanced due to VDA injection 3 days after MHT and lasted up to at least 7 days after MHT (Figures 5a and 5b). The difference between our results and those of Guo et al. [28] or Gao et al. [29] may be mainly due to the difference in the injection route of the agents and/or the affinity of the agents with tumor cells. When MNPs were injected intravenously, their clearance rate from the tumor might be faster than that when they were directly injected into the tumor. Further studies are necessary to elucidate the reason for the above difference.

Conclusion

We demonstrated that administration of VDA induced a reduction of tumor blood flow and delayed the tumor volume growth at an early stage after the injection of VDA. We also demonstrated that VDA enhanced the retention of MNPs in the tumor 3 to 7 days after MHT. These results suggest that VDA will be useful for enhancing the therapeutic effect of MHT when applied repeatedly. Our results also suggest that MPI is useful for quantitative evaluation of the tumor response to therapeutic agents such as VDA.

Acknowledgements

This work was supported by a Grant-in-Aid for Scientific Research (Grant No. 25282131) from the Japan Society for the Promotion of Science (JSPS). The authors are grateful to Prof. Masato Ohmi of Osaka University for his help in measuring tumor blood flow using a laser Doppler flow meter.

Declaration of Interest

The authors report no conflicts of interest.

References

1. Siemann DW (2011) The unique characteristics of tumor vasculature and preclinical evidence for its selective disruption by tumor-vascular disrupting agents. Cancer Treat Rev 37: 63-74.
2. Soignet SL, Maslak P, Wang ZG, Jhanwar S, Calleja E, et al. (1998) Complete remission after treatment of acute promyelocytic leukemia with arsenic trioxide. N Engl J Med 339: 1341-1348.
3. Li YM, Broome JD (1999) Arsenic targets tubulins to induce apoptosis in myeloid leukemia cells. Cancer Res 59: 776-780.
4. Lew YS, Brown SL, Griffin RJ, Song CW, Kim JH (1999) Arsenic trioxide causes selective necrosis in solid murine tumors by vascular shutdown. Cancer Res 59: 6033-6037.
5. Abe M, Hiraoka M, Takahashi M, Egawa S, Matsuda C, et al. (1986) Multi-institutional studies on hyperthermia using an 8-MHz radiofrequency capacitive heating device (Thermotron RF-8) in combination with radiation for cancer therapy. Cancer 58: 1589-1595.
6. Ito A, Honda H, Kobayashi T (2006) Cancer immunotherapy based on intracellular hyperthermia using magnetite nanoparticles: a novel concept of "heat-controlled necrosis" with heat shock protein expression. Cancer Immunol Immunother 55: 320-328.
7. van der Zee J (2002) Heating the patient: a promising approach ? Ann Oncol 13: 1173-1184.
8. Overgaard J (1980) Simultaneous and sequential hyperthermia and radiation treatment of an experimental tumor and its surrounding normal tissue *in vivo*. Int J Radiat Oncol Biol Phys 6: 1507-1517.
9. Haas GP, Klugo RC, Hetzel FW, Barton EE, Cerny JC (1984) The synergistic effect of hyperthermia and chemotherapy on murine traditional cell carcinoma. J Urol 132: 828-833.
10. Matsumoto K, Yamamoto N, Hagiwara S, Saito M, Furne H, et al. (2011) Optimization of hyperthermia and dendritic cell immunotherapy for squamous cell carcinoma. Oncol Rep 25: 1525-1532.
11. Griffin RJ, Lee AH, Rood KL, Stewart MJ, Lyons JC, et al. (2000) Use of arsenic trioxide as an antivascular and thermosensitizing agent in solid tumors. Neoplasia 2: 555-560.
12. Kumar CS, Mohammad F (2011) Magnetic nanomaterials for hyperthermia-based therapy and controlled drug delivery. Adv Drug Deliv Rev 63: 789-808.
13. Petryk AA, Giustini AJ, Gottesman RE, Trembly BS, Hoopes PJ (2013) Comparison of magnetic nanoparticle and microwave hyperthermia cancer treatment methodology and treatment effect in a rodent breast cancer. Int J Hyperthermia 29: 819-827.
14. Gleich B, Weizenecker J (2005) Tomographic imaging using the nonlinear response of magnetic particle imaging. Nature 435: 1214-1217.
15. Murase K, Hiratsuka S, Song R, Takeuchi Y (2014) Development of a system for magnetic particle imaging using neodymium magnets and gradiometer. Jpn J Appl Phys 53: 067001.
16. Murase K, Banura N, Mimura A, Nishimoto K (2015) Simple and practical method for correcting the inhomogeneous sensitivity of a receiving coil in magnetic particle imaging. Jpn J Appl Phys 54: 038001.
17. Murase K, Song R, Hiratsuka S (2014) Magnetic particle imaging of blood coagulation. Appl Phys Lett 104: 252409.
18. Murase K, Oonoki J, Takata H, Song R, Angraini A, et al. (2011) Simulation and experimental studies on magnetic hyperthermia with use of superparamagnetic iron oxide nanoparticles. Radiol Phys Technol 4: 194-202.
19. Biederer S, Knopp T, Sattel TF, Ludtke-Buzug K, Gleich B, et al. (2009) Magnetization response spectroscopy of superparamagnetic nanoparticles for magnetic particle imaging. J Phys D: Appl Phys 42: 205007.
20. Murase K, Aoki M, Banura N, Nishimoto K, Mimura A, et al. (2015) Usefulness of magnetic particle imaging for predicting the therapeutic effect of magnetic hyperthermia. Open J Med Imaging 5: 85-99.
21. Kuboyabu T, Yabata I, Aoki M, Banura N, Nishimoto K, et al. (2016) Magnetic particle imaging for magnetic hyperthermia treatment: visualization and quantification of the intratumoral distribution and temporal change of magnetic nanoparticles *in vivo*. Open J Med Imaging 6: 1-15.

22. Bettaieb A, Averill-Bates DA (2015) Thermotolerance induced at a mild temperature of 40°C alleviates heat shock-induced ER stress and apoptosis in HeLa cells. Biochim Biophys Acta 1853: 52-62.

23. Tozer GM, Kanthou C, Baguley BC (2005) Disrupting tumour blood vessels. Nat Rev Cancer 5: 423-435.

24. Hines-Peralta A, Sukhatme V, Regan M, Signoretti S, Liu ZJ, et al. (2006) Improved tumor destruction with arsenic trioxide and radiofrequency ablation in three animal models. Radiology 240: 82-89.

25. Shen ZY, Zhang Y, Chen JY, Chen MH, Shen J, et al. (2004) Intratumoral injection of arsenic to enhance antitumor efficacy in human esophageal carcinoma cell xenografts. Oncol Rep 11: 155-159.

26. Kusakabe Y, Miyazaki S, Tachibana A, Matsuura R, Matsuura N, et al. (2009) Development of a method to quantitatively monitor the effect of inhibition of nitric oxide synthase on tumour vascular activity using dynamic contrast-enhanced computed tomography. J Med Eng Technol 33: 460-469.

27. Tozer GM, Prise VE, Lewis G, Xie S, Wilson L, et al. (2009) Nitric oxide synthase inhibition enhances the tumor vascular-damaging effects of combretastatin A-4 3-O-phosphate at clinically relevant doses. Clin Cancer Res 15: 3781-3790.

28. Guo N, Zhang F, Zhang X, Guo J, Lang L, et al. (2015) Quantitative evaluation of tumor early response to a vascular-disrupting agent with dynamic PET. Mol Imaging Biol 17: 865-873.

29. Gao M, Yao N, Huang D, Jiang C, Feng Y, et al. (2015) Trapping effect on a small molecular drug with vascular-disrupting agent CA4P in rodent H22 hepatic tumor model: *in vivo* magnetic resonance imaging and postmortem inductively coupled plasma atomic emission spectroscopy. J Drug Target 23: 436-443.